15th International Symposium on Computer Methods in Biomechanics and Biomedical Engineering
and
3rd Conference on Imaging and Visualization
CMBBE 2018
P. R. Fernandes and J. M. Tavares (Editors)

Prediction of Osteophytes relevance in Human Osteoarthritic Femur Head from Load pattern rearrangement Simulations: an Integrated FEM Study

Fabiano Bini[1], Andrada Pica[1], Andrea Marinozzi[2], Franco Marinozzi[1]

[1]Department of Mechanical and Aerospace Engineering, "Sapienza" University of Rome,
via Eudossiana, 18–00184 Rome, Italy
fabiano.bini@uniroma1.it, andrada.pica@uniroma1.it, franco.marinozzi@uniroma1.it

[2]Orthopedy and Traumatology Area, "Campus Bio-Medico" University,
via Alvaro del Portillo, 200-00128 Rome, Italy
A.Marinozzi@unicampus.it

Keywords: Hip osteoarthritis, Osteophytes, Geodes, 3D-FEM model, Load pattern

Introduction: Osteoarthritis (OA) is the most common degenerative joint disease and it is mainly characterized by articular cartilage damage, synovial fibrosis and osteophyte formation. Osteophytes are osteo-cartilaginous outgrowths that involve the bone structure of osteoarthritic joints. In this study we analyzed how osteophytes evolution leads to a rearrangement of the stresses and strains within the subchondral trabecular bone.

Methods: A 3D, isotropic, homogeneous and linearly elastic model of the proximal half of the human femur head was implemented from radiographic images. The osteophytes formation is achieved by introducing different loading distributions that mimic concentrated loads on the femur head surface. By means of the finite element analysis (FEA), we explored the circumstance that osteophytes growth alters the physiological load pattern in such a way that large zones of reduced load can cause resorption and the formation of bone cysts (geodes), surrounded by areas of overstimulated tissue (eburnation).

Results: The outcome of the FEA provides Von Mises (VM) Stress and strain energy density (SED) for four different scenarios (Healthy, Early, Intermediate and Advanced Osteoarthritis) characterized by different osteophytes spatial distributions on the femur head. According to our simulation, osteophytes growth leads to abnormal contact between bony extremities and alters loading conditions in the femoral head which in turn will induce the re-arrangement of trabecular subchondral bone. The simulations of VM stresses and SED were compared to clinical studies to validate the effectiveness of the model.

Conclusion: The parametric study conducted can result particularly useful not only for the clinical assessment of bone failure but also for the design of patient-specific scaffold, especially if combined with 3D-printing technique.

1 INTRODUCTION

Osteoarthritis (OA) is a debilitating joint disorder with an exponentially increasing incidence after the age of 50. It represents a significant and expensive issue in the public health. In fact, with the increase of aging population, OA is expected to become the fourth leading cause of disability by 2020 [1]. Therefore, it emerges the crucial importance to better understand the disease progression and to predict the structural consequences of the joint degradation.

Generally, OA is characterized by progressive cartilage degeneration, alteration of subchondral bone structure, osteophytes formation and synovial fibrosis [2]. Although it is often described as an articular cartilage disease, new evidence highlights that changes of the structural and material properties of bone are not secondary manifestations of OA, but active contributors to the disease progression. Altered load distributions can accelerate the evolution of OA [3] and lead to the aberrant remodelling processes of the joint functional units.

The importance of bone alterations in OA progression is still not properly understood. During the OA development, detectable alterations in the composition and structure of bone tissue appear earlier than cartilage degeneration [4]. Therefore, it is worth investigating the bone variations in order to achieve an early identification of the disease. The OA alterations in bone include increases of subchondral cortical bone thickness, decreases in subchondral trabecular bone mass, formation of osteophytes and cysts [4]. Osteophytes are osteo-cartilaginous outgrowths that promote the formation of contact points between the bony extremes of osteoarthritic joints and participate to the development of mechanical forces alterations within the diseased articulations [5-7]. Osteophytes are developed by a process of endochondral ossification, already observed in the primary osteogenesis [4]. This mechanism of bone formation is characterized by a rapid and unorganized mineralization of the cartilaginous matrix [8].

Osteophytes develop at sites of tendon insertion or they arise from the periosteum covering the bone [9]. Radiographic histological study [5] has identified different distribution of osteophytes, i.e. in the peripheral zone of the femoral head (marginal osteophytes), on the medial surface of the femoral head (epiarticular osteophytes) and across the basal layers of the articular cartilage (subarticular osteophytes). In this study, depending on the OA severity, we analysed the scenarios of marginal, epiarticular and subarticular osteophytes developed on the human femur head.

Different hypotheses have been advanced towards the role of osteophytes in the evolution of OA. Some studies [10-11] illustrate the formation of osteophytes as an adaptive response of the joint to redistribute the load on the articular surface and to prevent cartilage degeneration. Conversely, osteophytes are considered as a pathological side effect of the bone remodelling process in conditions of aberrant joint variations [12].

Previous studies [13-14], based on a 2D finite element model of the femur head, give insights into the alterations of the strain and stress distribution subsequent to the development of osteophytes. In the current investigation, we analyse a 3D model of the femur head in healthy and osteoarthritic situations, subject to the loading conditions of the stance phase of gait. The aim of this study is to explore the response of the trabecular bone in terms of Von Mises (VM) stress and strain energy density (SED) to the altered load distribution caused by the osteophytes presence. The mechanical behaviour of the healthy hip joint is used as a reference for the evaluation of three different OA severity stages, namely Early, Intermediate and Advanced Osteoarthritis. Furthermore, the drastically changes within the trabecular bone achieved through the FEM simulation are compared with clinical results.

2 METHODS

A 3D model of the proximal half of the femur head was implemented from Computer Tomography images. The image slices of the femur head of a 72 years old male were provided by the National Library of Medicine in Maryland (USA). The 3D FEM model is characterized as a multilayer solid, composed of an inner trabecular region, an external cortical zone and a cartilage shell which covers the femoral head [15-16]. The radius of the femur head is found by calculating the radius of the circle that best fits the contour of the femoral head. It was obtained, therefore, a value of 24 mm. In the present study, cartilage thickness is maintained constant at 2.5 mm on the whole surface of the femoral head. Since it was observed that osteophytes formation can occur without overt cartilage damage [17], we also assume that the cartilage thickness remains unaltered during OA evolution.

Materials were assumed to be constant, linearly elastic and isotropic. From related literature, we set the numerical values of their physical properties. The trabecular tissue is characterized by a Young modulus of 1 GPa [18-20], a Poisson's ratio of 0.3 [21] and an apparent tissue density of 1000 kg/m^3 [22]. For the cortical bone, a Young modulus of 22 GPa [23], a Poisson's ratio of 0.3 [24] and a tissue density equal to 2000 kg/m^3 [25] is assigned. The articular cartilage is assumed to have an average value of the Young modulus equal to 15 MPa [26], a Poisson's ratio of 0.1 [27] and a density of 1000 kg/m^3 [3]. The above numerical considerations remain unchanged for both healthy and pathological models. Appropriate boundary conditions allow to highlight the evolution of the disease.

The study concerns four scenarios of the 3D femur model: a healthy femur condition (HF) and three different levels of OA severity, i.e. early stage (ES), intermediate stage (IS) and advanced stage (AS). The ES condition is characterized by the presence of two groups of marginal osteophytes (O_1 and O_2). In the IS model, a foveal group of osteophytes (O_3) is added to the existing peripheral groups. The AS case is represented by four groups of osteophytes, namely two marginal osteophytes, an epiarticular (O_3) and a subarticular (O_4) bony outgrowths (O_4).

Finite element analysis of the 3D model is performed with Comsol Multiphysics 5.0 (COMSOL – Stockholm, Sweden). The centre of the Cartesian coordinate system coincides with the centre of the femur head. The femoral Z-axis is vertical, the Y-axis points in the medial-lateral direction and the X-axis points in the postero-anterior direction. The Y and Z-axes are in the coronal plane of the femur, while the X-axis is in the sagittal plane.

In order to represent the evolution of the disease in the FEM model, the variations of geometrical parameters concerning the acetabular coverage of the femoral head and different load distributions are taken into account. The load is transferred between the acetabulum and the femur head by means of the contact surface defined by three centre-edge angles: the centre-edge angle of Wiberg in the YZ plane, the anterior ($\theta_{A\text{-}CE}$) and posterior ($\theta_{P\text{-}CE}$) centre edge angles in the sagittal plane, i.e. XZ plane [28] (Fig. 1). The extension of the main contact area (MCA) in the YZ plane is identified by the functional angle θ_F. In the HF condition, the centre edge angle of Wiberg (θ_{CE}) in the YZ plane is assumed to be equal to 30°, while the angle θ_F is set to 110°. Generally, the pathological cases are characterized by values of θ_{CE} minor than 20° [29], thus we adopted a value of 10° in the OA models. In the coronal plane, we assume that the presence of osteophytes acts in detriment of the extension of the MCA. Thus, we make the hypothesis that in the ES model the functional angle θ_F is equal to 50°, in the IS model θ_F is set to 40° while in the AS case θ_F is 35°. Conversely, the surface occupied by each group of osteophytes increases with the degeneration of the disease. We make the assumption that the osteophytes characterizing an OA stage have the extension

defined by the angle θ_{Oi}. Namely, the ES model is defined by the angle θ_{Oi} equal to 15°, in the IS model θ_{Oi} is set to 20°, while in the AS model θ_{Oi} is 25°.

In the sagittal plane, the extension of the MCA is maintained constant, both in healthy and pathological conditions. Furthermore, we assume that the groups of osteophytes have the same extension as the MCA. According with clinical observation [28], we set both $\theta_{A\text{-}CE}$ and $\theta_{P\text{-}CE}$ to 60°.

In the single legged stance phase of gait, the loading force (H) acting on the hip joint is determined by the partial body mass (W), obtained as total body mass diminished by the weight-bearing leg, and the abductor muscle force calculated to be two times W [30]. The magnitude of H is approximatively 2.4 times W, in agreement with [31]. For a patient with a body mass estimated to 65 kg, the loading force H corresponds around 1554 N.

The resultant force H acting between the acetabulum and the femur head was directed normally to the contact surface of the femur head. Furthermore, the synovial fluid between the bone and the cartilage plays a role of lubrification, therefore tangential stresses due to friction were ignored. In the HF, the total force H acts on the contact surface between the acetabulum and the femur head, i.e. MCA. In pathological conditions, the force is distributed among various contact regions, namely the reduced MCA and the different groups of osteophytes. In accordance with [13-14], in the ES, IS and AS models, the load acting on the MCA is respectively 75%, 50% and 25% of the total amount H. The remaining percentages were equally distributed between the two, three and four groups of osteophytes which characterize the OA level of severity.

Normal and pathological biomechanical conditions were simulated implementing different loading patterns in order to obtain contact pressure distribution during the stance phase of gait. We applied the load profile as a boundary condition on each domain that composes the contact surface in the FE model of the femur head. In the coronal plane, we divided the contact surface in circular sectors characterized by a centre-edge angle of 5°. Globally, the contact pressure (p) integrated over the articular contact surface (A) is equal to the force H transmitted to the hip joint, as indicated by the following integral relationship [32]:

$$\int \boldsymbol{p} \cdot \boldsymbol{dA} = \boldsymbol{H} \tag{1}$$

The real hip joint is characterized as a ball and socket configuration. In order to model the transmission of force across the hip joint, we consider different pressure patterns in the healthy and OA conditions [33-34]. In the HF condition, the pressure distribution within the hip joint in the YZ plane could be described by a cosine distribution, as indicated by Eq. (2) [32, 35]:

$$\boldsymbol{p} = \boldsymbol{p}_{\max} \cdot \cos \boldsymbol{\gamma} \tag{2}$$

where p_{max} is the maximum contact pressure and γ is the angle between a generic point on the MCA and the Z-axis. The maximum pressure is calculated as follows:

$$\boldsymbol{p}_{\max} = \frac{\boldsymbol{H}}{\sum_{\boldsymbol{i}=1}^{\boldsymbol{n}} \cos(\boldsymbol{\gamma}_{\boldsymbol{i}})} \cdot \frac{1}{\boldsymbol{A}} \tag{3}$$

where γ_i is the value of the angle γ at the distal extremity of each domain of the MCA from the Z-axis, n is the number of the domains and A is the area of the contact surface.

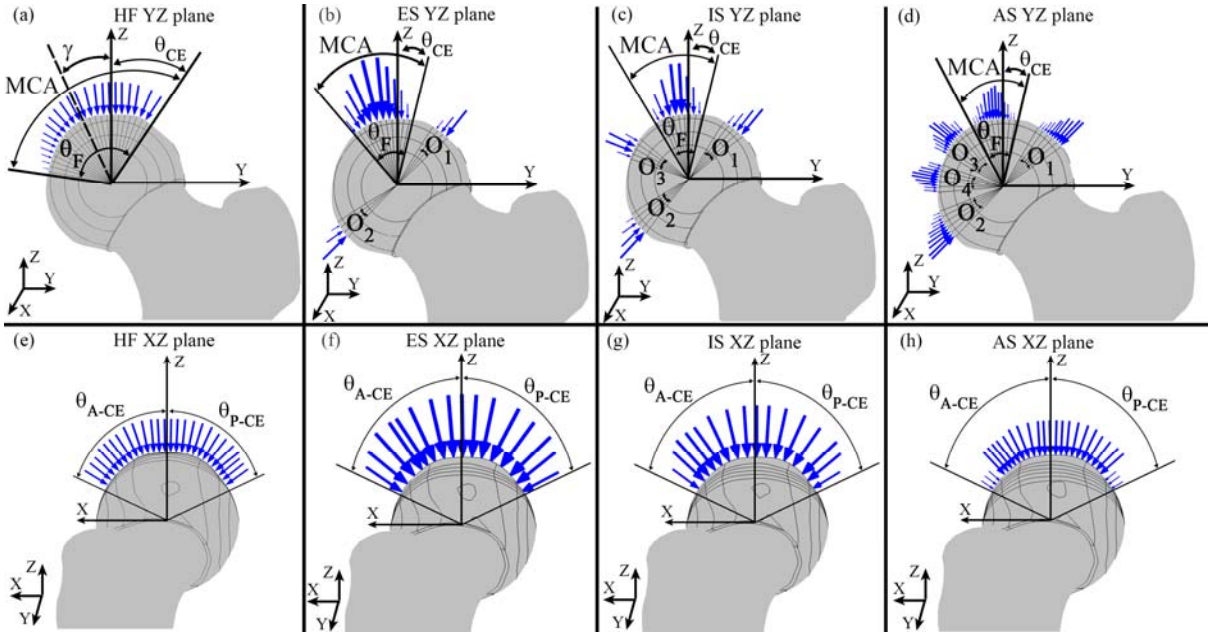

Figure 1: Load distribution in the YZ plane, i.e. coronal plane, in the healthy femur (HF) (a), in the ES (b), in the IS (c) and in the AS (d) models of the OA femur. From (e) to (h), the load distributions in the XZ plane, i.e. sagittal plane, are illustrated for HF, ES, IS and AS models respectively. For each plane, we represent the load distribution of the most solicited sections, which are sited in correspondence of the coordinate system origin. The blue arrows are proportional with the load magnitude.

In pathological cases, concentrated loads are supposed to be experimented by the femoral head surface because of the osteophytes appearance and the reduction of the MCA. In reviewing the literature associated with contact interaction [34, 36-37], the pressure pattern due to the load transfer on the femur head via the thin elastic layer of the cartilage is modelized with a symmetric parabolic distribution. According to Johnson [34], the pressure distribution can be described as a function of the distance $\boldsymbol{r}$ from the centre of the contact area of radius $\boldsymbol{a}$ as expressed by Eq. (4) [34,36], where p_{max} is the maximum contact pressure:

$$\boldsymbol{p}(\boldsymbol{r}) = \boldsymbol{p}_{\max} \cdot \left[1 - \left(\frac{\boldsymbol{r}}{\boldsymbol{a}} \right)^2 \right]^{\frac{1}{2}} \tag{4}$$

The maximum contact pressure is expressed as:

$$\boldsymbol{p}_{\max} = \frac{\boldsymbol{k} \cdot \boldsymbol{H}}{\boldsymbol{A}} \tag{5}$$

where the coefficient k indicates the percentage of the total force H which acts on the contact area A. The latter can be referred to the reduced MCA or to the contact surface of the osteophytes.

The pressure distributions acting on the reduced MCA, on the foveal, epiarticular and subarticular osteophytes are described by the axysymmetrical parabolic profile described previously. The maximum pressure value occurs in the centre of the contact area and null in the peripheral zone, at the maximum distance from the centre.

The marginal osteophytes are characterized as half spheres impinging on the acetabular labrum. In order to respect the acetabular coverage conditions, we considered a half parabolic distribution in the YZ plane. Therefore, the maximum pressure is obtained in correspondence

of the acetabular rim in agreement with [38] that indicate this region as one of the most solicitated of the femur head.

In the sagittal plane, for both healthy and pathological models, we adopt a symmetric parabolic distribution of the pressure on the femur head. The maximum value is achieved in the centre of the contact surface, which is assumed to be in correspondence of the Z-axis [37] (Fig. 1 e-h)

In order to reduce the computational costs, the mesh of the FE model was chosen finer in the region of the femoral head and coarser in the remaining part of the model. The details of the mesh generation are given in Table 1.

To assess the bone tissue response for each loading case, the equivalent VM stress and the SED are calculated. Equivalent VM stress is calculated as follows (Eq. 6):

$$\sigma_{VM} = \sqrt{\frac{1}{2}\left[(\sigma_1 - \sigma_2)^2 + (\sigma_2 - \sigma_3)^2 + (\sigma_1 - \sigma_3)^2\right]} \tag{6}$$

where σ_1, σ_2 and σ_3 are the principal stresses. SED is obtained according to Eq. (7):

$$SED = \frac{1}{2}(\sigma_{xx} \cdot \varepsilon_{xx} + \sigma_{yy} \cdot \varepsilon_{yy} + \sigma_{zz} \cdot \varepsilon_{zz}) + (\sigma_{xy} \cdot \varepsilon_{xy} + \sigma_{xz} \cdot \varepsilon_{xz} + \sigma_{yz} \cdot \varepsilon_{yz}) \tag{7}$$

where σ_{ii}, σ_{ij}, ε_{ii} and ε_{ij} are the stress and strain components, respectively.

3 RESULTS AND DISCUSSION

The present work investigates the rearrangement of stress and strain patterns subsequent to the altered load distribution associated with OA progression. Although FEM simulations interested the proximal half of the femur, the following analysis focuses particularly on the region of the femoral head. We investigated the equivalent stress distribution, VM stress and, the SED for the three layers composing the 3D FEM model, i.e. cartilage, cortical and trabecular bone. We analyse parallel slices to the anatomical planes, i.e. coronal plane (YZ plane), sagittal plane (XZ plane) and transversal plane (XY plane), in correspondence of the most solicitated regions. In the coronal and sagittal planes, the slices analysed are localized in the coordinate system origin, while in the transversal plane, the slice of interest is sited at a distance R = 13 mm on the negative Z-axis direction with respect to the coordinate system origin (Fig. 2).

To the best of our knowledge, this is the first 3D FE study of the femur head that investigates the trabecular bone structure during OA evolution. In Fig. 3a-d, the VM stress relating to the coronal plane is illustrated. The stress patterns achieved in the present study result in accordance with previous outcomes from 2D finite element analysis

Table 1: Statistics of FE simulations

Model	Degrees of freedom	Number of mesh elements	Minimum mesh element
HF	19582908	4833517	10 μm
ES	1823022	443255	5 μm
IS	1565646	378836	10 μm
AS	11441082	2822441	5 μm

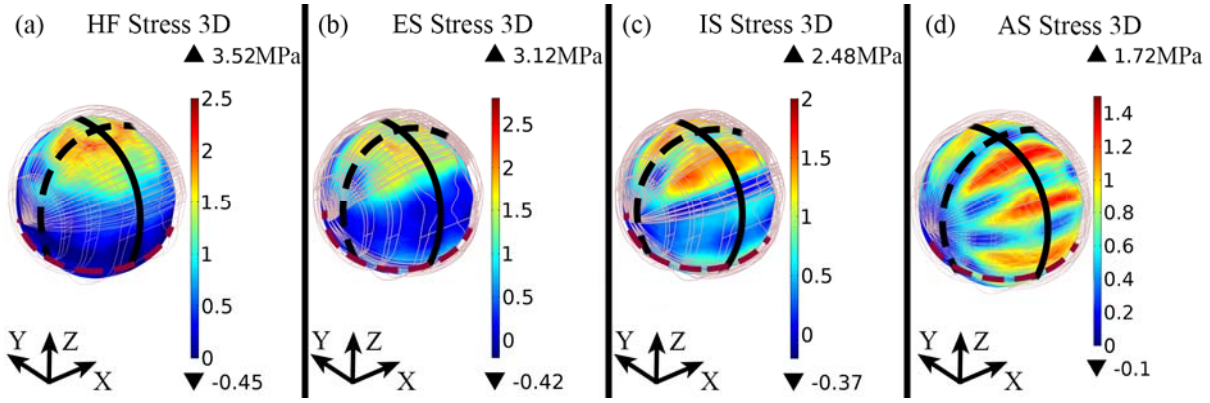

Figure 2: Stress distribution in the trabecular region of the HF (a), ES (b), IS (c) and AS (d) models of the femoral head. The lighter grey shell corresponds to the cortical bone and the cartilage geometry. The continuous black line represents the parallel slice to the YZ plane (coronal plane), the dotted black line indicates the parallel slice to the XZ plane (sagittal plane) and the dotted dark red line illustrates the parallel slice to the XY plane (transversal plane), that are analysed in Fig. 3 and 4.

performed by [13-14]. The maximum value of VM stress is observed in the cortical region, whilst in the trabecular bone, elevated VM stress is identified in the femoral neck zone and also in correspondence of the reduced MCA in the OA cases. In addition, the subchondral bone shows a peculiar pattern with an alternation of overstressed and low stressed regions in the OA models. In agreement with Wolff's law [39], a high turnover of bone tissue is identified in stimulated zones, while understressed regions enable the appearance of geodes [23]. Subchondral sclerosis is commonly reported in OA patients and it is widely considered a main feature of advanced OA [5, 40-41]. Abnormal structures are highlighted also by the vector maps of the direction of strain within the trabecular tissue. In fact, changes in the direction of the strain vectors are observed in the understimulated zones where bone geodes are supposed to develop.

Overall, the structural variations are noticeable higher with the OA evolution. With respect to the HF outcomes, suitable conditions for cysts generation are observed also in the sagittal plane of the OA models (Fig. 3 f-h). We achieved roughly the same VM stress values in both coronal and sagittal planes. In the trabecular bone, the highest stress is denoted in the femoral neck region, whilst localized points of medium stress are sited in the superior femoral region. In the intermediate and advanced condition of the pathology, in the subchondral bone region, an extended zone is characterized by a low value of VM stress, which represents a favourable site for geodes development [6, 41].

In the transverse plane (Fig. 3 i-n), FEM simulations highlighted areas with elevated VM stress in correspondence of the cortical tissue and the trabecular region of the femoral neck, as it occurs also in the previous two planes investigated. Nonetheless, favourable conditions for bone sclerosis are not identified. In fact, a gradual transition from high to low stress could be noted, differently from the alternated pattern achieved in the other planes.

In the subchondral trabecular bone, OA is associated with an abnormal low mineralization pattern [2]. The presence of osteophytes leads to a critical load distribution which induces an altered remodelling response. This is well corroborated also by the SED distribution (Fig. 4). When compared with the healthy model, the SED largest value achieved in the trabecular region decreases with the progression of the disease. In all models, high SED values are visible at the femoral neck zone of the trabecular tissue, while in the OA conditions, an additional region of elevated SED is visible in correspondence of the MCA.

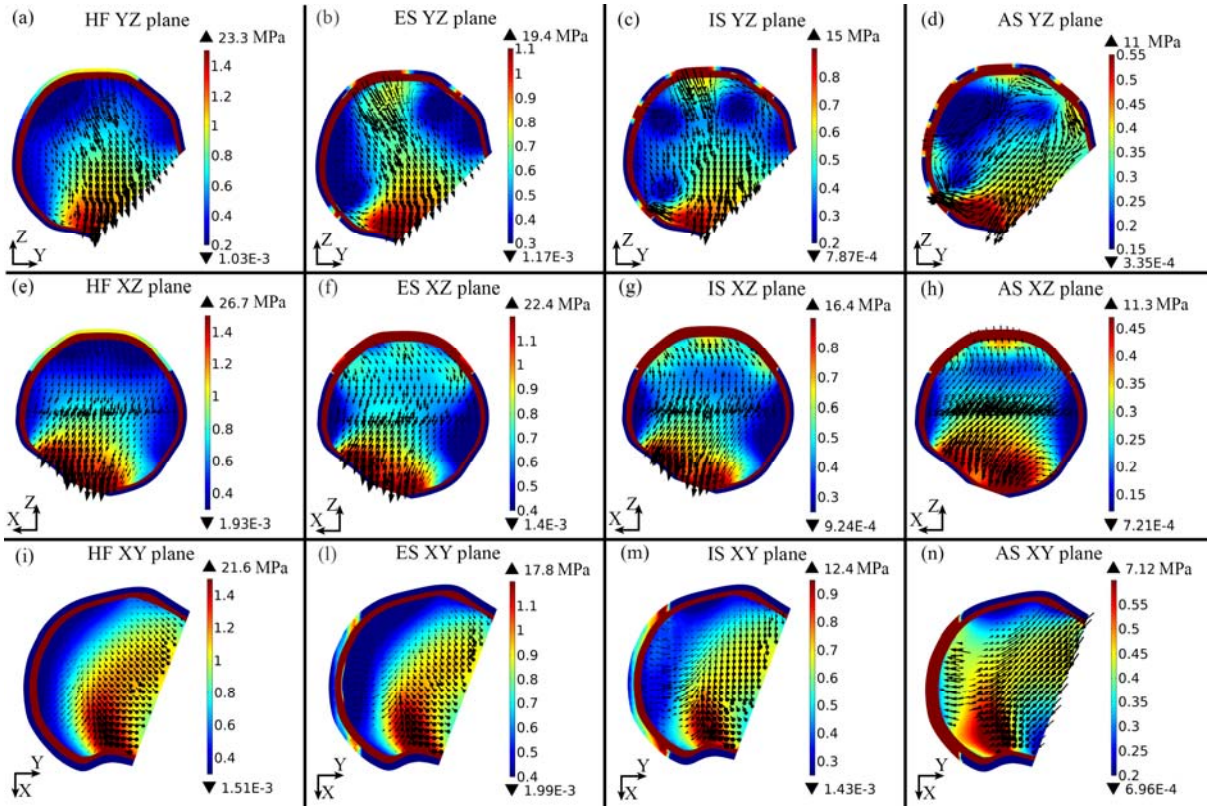

Figure 3: Von Mises stress distribution and vector maps of strain direction in the YZ plane (coronal plane) (a-d), in the XZ plane (sagittal plane) (e-h) and in the XY plane (transversal plane) (i-n) of the four models, i.e healthy case (HF), early stage (ES), intermediate stage (IS) and advanced stage (AS) of the OA femur.

In the IS and AS models, zones with low values of SED that generate the condition for geodes development are identified in both coronal and sagittal planes of the subchondral bone. Since the SED is an indicator of the mechanical stimulus sensed by the osteocytes to govern bone remodelling phenomena [3], this pattern leads to an increase of the bone material characterized by a lower mineralization as observed also by other studies [13,14,23]. Clinical studies [5,7,40] delineated that cavitary lesions in bone structure are encountered individually under the surface of cortical bone or in pairs directly opposing each other. In the present study, the first condition is identified in the coronal plane sections, while the second localization is observed prevalently in the sagittal plane sections.

The values of VM stress and SED achieved in the present study were corroborated with the results obtained by previous researches [23,42]. These outcomes allow to determine the validity of the loading conditions applied on the MCA and in correspondence of the osteophytes in both, coronal and sagittal planes. Furthermore, also the localization of appropriate sites for geodes development achieved from the FE simulations confirms the suitability of the loading pattern considered.

However, as a final remark we want to point out some limitations of the current analysis. In the present 3D study, we considered the thickness cartilage to be constant in the healthy and OA situations. This assumption is supported by recent investigation that highlights the existence of bone alterations in absence of cartilage damage [15]. However, predictions considering different cartilage thickness should be further compared and its importance could be emphasized in such case. Since Van Rietbergen et al. [23] reported no significant changes

in bone tissue material properties between healthy and disease conditions, we considered constant values of density and Young's module. We also adopted the hypothesis that bone

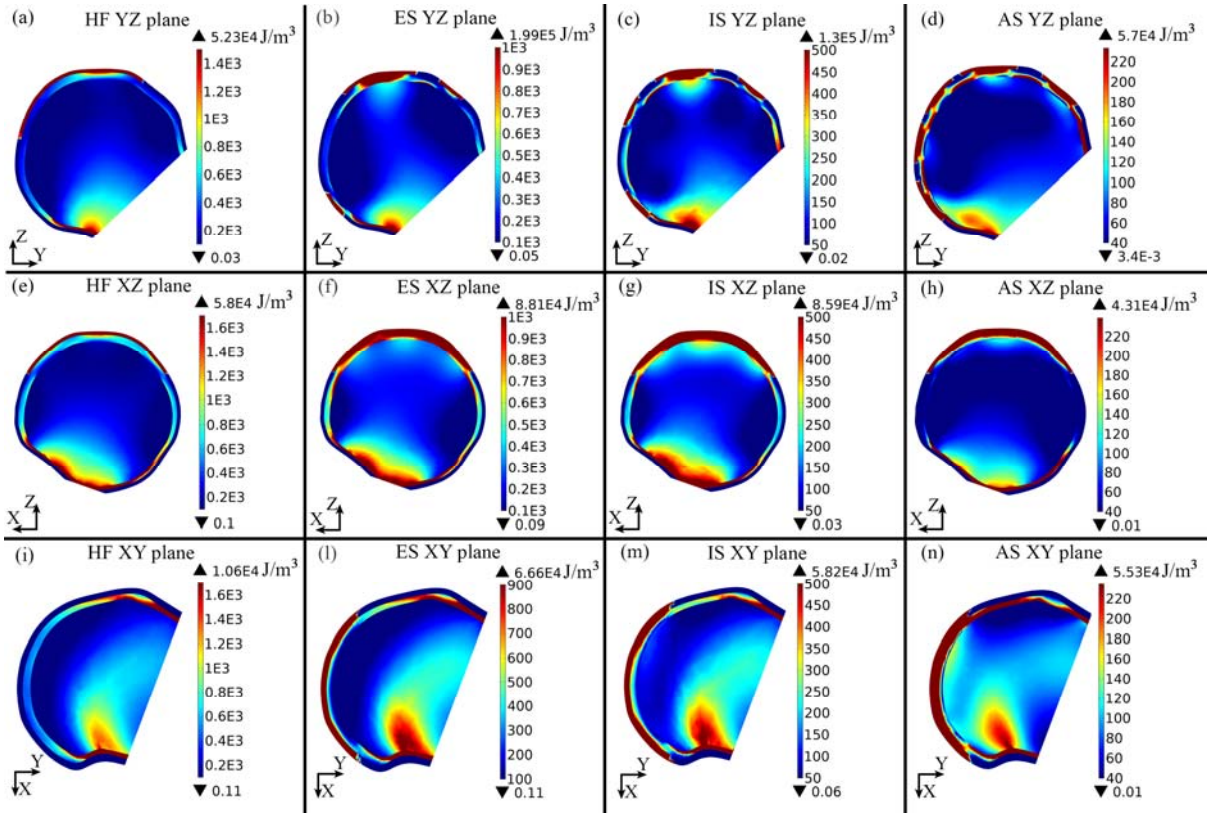

Figure 4: SED distribution in the YZ plane (coronal plane) (a-d), in the XZ plane (sagittal plane) (e-h) and in the XY plane (transversal plane) (i-n) of the four models, i.e healthy case (HF), early stage (ES), intermediate stage (IS) and advanced stage (AS) of the OA femur.

tissue exhibits linear, elastic, homogeneous, isotropic behaviour. Although this approach is not physiologic, it was demonstrated previously that heterogeneous tissue mineralization has a minor effect on apparent trabecular bone elastic properties [43].

4 CONCLUSIONS

Subchondral bone plays a pivotal role in the pathogenesis of OA, manifesting microarchitectural variations [2]. In the present study, the effect of OA on the variation of the subchondral trabecular bone in the femoral head was examined by means of FEM simulations. The analysis of the outcomes confirms the hypothesis that abnormal load distribution due to the presence of osteophytes could lead to the development of bone sclerosis in the subchondral trabecular bone. This tendency was validated through VM stress and SED pattern, that show low values in the subchondral bone.

The results, in agreement with the previous studies of [13-14], indicate that FEM simulations could be used as a marker of the variation of subchondral bone in the femur head. The outcomes provide refined insight to femoral head structure and mechanical response to different loading patterns that could improve knowledge in the evolution of OA. Identification of potential mechanism acting in the OA bone variations can result particularly

useful not only for the clinical assessment of bone failure. We also believe that the present work can be a valuable support to the design of extracellular matrix-like scaffolds for bone tissue engineering to optimize the transport phenomena [44-45], the mechanical properties of bone substitutes, especially if combined with biosensors based on ZnO nanomaterials [46-47] and 3D-printing technique.

REFERENCES

[1] A.D. Woolf, B. Pfleger. Burden of major musculoskeletal conditions. *Bull World Health Organ*, **81**(9), 646-656, 2003.

[2] G. Li, J. Yin, J. Gao, T. S. Cheng, N.J. Pavlos, C. Zhang, M.H. Zheng. Subchondral bone in osteoarthritis: insight into risk factors and microstructural changes. *Arthritis Research & Therapy*, **15**, 223, 2013.

[3] L.G.E. Cox, B. Van Rietbergen, C.C. Van Donkelaar, K. Ito. Bone structural changes in osteoarthritis as a result of mechanoregulated bone adaptation: a modelling approach. *Osteoarthritis and cartilage*, **19**, 676-682, 2011.

[4] S.R. Goldring S.R. Alterations in periarticular bone and cross talk between subchondral bone and articular cartilage in osteoarthritis. *Ther Adv Musculoskel Dis*, **4**(4), 249-258, 2012.

[5] A.K. Jeffery. Osteophytes and the osteoarthritic femoral head. *The Journal of bone and joint surgery*, **57**(3), 1975.

[6] T.D. Turmezei and K.E.S. Poole. Computed tomography of subchondral bone and osteophytes in hip osteoarthritis: the shape of things to come? *Frontiers in endocrinology*, **2**, Article 97, 2011.

[7] T.D. Turmezei, D.J. Lomas, M.A. Hopper, K.E.S. Poole. Severity mapping of the proximal femur: a new method for assessing hip osteoarthritis with computed tomography. *Osteoarthritis Cartilage,* **22**, 1488-1498, 2014.

[8] M.J. Olstza, X. Cheng, S.S Jee, R. Kumar, Y.Y Kim, M.J. Kaufman, E.P. Douglas, L.B. Gower. Bone structure and formation: a new perspective. *Mat Sci Eng R* **58**, 77–116, 2007.

[9] E.N. Blaney Davidson, E.L. Vitters, H.M. Van Beuningen, F.A.J. Van de Loo, W.B. Van den Berg, P.M. Van der Kraan. Resemblance of osteophytes in experimental osteoarthritis to transforming growth factor β-induced osteophytes. *Arthritis Rheumatism*, **56**(12), 4065-4073, 2007.

[10] P. Neuman, A. Hulth, B. Lindén, O. Johnell, L. Dahlberg. The role of osteophytic growth in hip osteoarthritis". *International Orthopaedics (SICOT)*, **27**, 262–266, 2003.

[11] R.W. Moskowitz. Bone remodelling in osteoarthritis: subchondral and osteophytic responses. *Osteoarthritis and Cartilage*, **7**, 323–324, 1999.

[12] C-J. Menkes, N.E. Lane. Are osteophytes good or bad? *Osteoarthritis Cartilage*, **12**, S53–S54, 2004.

[13] F. Marinozzi, F. Bini, A. De Paolis, R. De Luca, A. Marinozzi. Effects of hip osteoarthritis on mechanical stimulation of trabecular bone: a finite element study. *J. Med. Biol. Eng.*, **35**(4), 535-544, 2015.

[14] F. Marinozzi, F. Bini, A. De Paolis, F. Zuppante, R. Bedini, A. Marinozzi. A finite element analysis of altered load distribution within femoral head in osteoarthritis.

Computer Methods in Biomechanics and Biomedical Engineering: Imaging & Visualization, **3**(2), 84-90, 2015.
[15] F. Marinozzi, A. Marinozzi, F. Bini, F. Zuppante, R. Pecci, R. Bedini. Variability of morphometric parameters of human trabecular tissue from coxo-arthritis and osteoporotic samples. *Ann. I. Super. Sanità*, **48**(1), 19-25, 2012.
[16] F. Marinozzi, F. Bini, A. Marinozzi, F. Zuppante, A. De Paolis, R. Pecci, R. Bedini. Technique for bone volume measurement from human femur head samples by classification of micro-CT image histograms. *Ann. I. Super. Sanità*, 49,(3), 300-305, 2013.
[17] P.M. Van der Kraan, W.B. Van den Berg. Osteophytes: relevance and biology. *Osteoarthritis and Cartilage*, **15**, 237-244, 2007.
[18] F. Bini, A. Marinozzi, F. Marinozzi and F. Patanè. Microtensile measurements of single trabeculae stiffness in human femur. *J. Biomech*. **35**, 1515–1519, 2002.
[19] F. Marinozzi, F. Bini, A. Marinozzi. Evidence of entropic elasticity of human bone trabeculae at low strains. *J. Biomech.* **44**(5), 988-991, 2011.
[20] G. Bini, F. Bini, R. Bedini, A. Marinozzi, F. Marinozzi. 2017. A Topological Look at Human Trabecular Bone Tissue. *Mathematical Biosciences*, 288(1), 159-165, 2017.
[21] A. Pustoc'h and L. Cheze. Normal and osteoarthritic hip joint mechanical behaviour: A comparison study. *Medical & Biological Engineering & Computing*, **47**, 375–383, 2009.
[22] S. Cowin. *Bone mechanics handbook*. Boca Raton (FL): CRC Press, 2001.
[23] B. Van Rietbergen, R. Huiskes, F. Eckstein, P. Ruegsegger. Trabecular bone tissue strains in the healthy and osteoporotic human femur. *J Bone Miner Res*, **18**(10), 1781–1788, 2003.
[24] E. Verhulp, B. Van Rietbergen and R. Huiskes. Load distribution in the healthy and osteoporotic human proximal femur during a fall to the side. *Bone*, **42**, 30–35, 2008.
[25] F. Marinozzi, A. De Paolis, R. De Luca, F. Bini, R. Bedini and A. Marinozzi. Stress and strain patterns in normal and osteoarthritic femur using finite element analysis. *Proceedings of CompImage-computational modelling of objects represented in images III: Fundamentals, methods and applications*, 247-250, 2012.
[26] F. Richard, M. Villars, S. Thibaud. Viscoelastic modelling and quantitative experimental characterization of normal and osteoarthritic human articular cartilage using indentation. *J. Mechanical behaviour of biomedical materials*. **24**, 41-52, 2013.
[27] K.A. Athanasiou, M.P. Rosenwasser, J.A. Buckwalter, T.I. Malinin, V.C. Mow. Interspecies comparisons of in situ intrinsic mechanical properties of distal femoral cartilage. *J. Orthop Res.*, **9**, 330-340, 1991.
[28] D. Miyasaka, T. Ito, N. Imai, K. Suda, I. Minato, Y. Dohmae, N. Endo. Three-dimensional assessment of femoral head coverage in normal and dysplastic hips: a novel method. *Acta Med. Okayama*, **68**(5), 277-284, 2014.
[29] Z. Miller, M.B. Fuchs, M. Arcan. Trabecular bone adaptation with an orthotropic material model. *J Biomech.*, **35**, 247–256, 2002.
[30] E. Genda, N. Konishi, Y. Hasegawa, T. Miura. A computer simulation study of normal and abnormal hip joint contact pressure. *Arch Orthop Trauma Surg*, **114**, 202-206, 1995.
[31] G. Bergmann, G. Deuretzbacher, M. Heller, F. Graichen, A. Rohlmann, J. Strauss, G.N. Duda. Hip contact forces and gait patterns from routine activities. *J. Biomech* **34**, 859-871, 2001.
[32] P. Brinckmann, W. Frobin, E. Hierholzer. Stress on the articular surface of the hip joint in healthy adults and persons with idiopathic osteoarthrosis of the hip joint. *J. Biomech* **14**(3), 149-156, 1981.

[33] F. Bachtar, X. Chen, T. Hisada. Finite element contact analysis of the hip joint. *Med Bio Eng Comput*, **44**, 643-651, 2006.
[34] K.L. Johnson. *Contact mechanics*. Cambridge: Cambridge University Press, 1985.
[35] A.S Greenwald, J.J. O'Connor. The transmission of load through the human hip joint. *J. Biomech,* **4**, 507-528, 1971.
[36] G.R. Naghieh, Z.M. Jin, H. Rahnejat. Contact characteristics of viscoelastic bonded layers. *Appl. Math. Modelling*, **22**, 569-581, 1998.
[37] X. Fang, C. Zhang, X. Chen, Y. Wang, Y. Tan. A new universal approximate model for conformal and non-conformal contact of spherical surfaces. *Acta Mach*, **226**, 1657-1672, 2015.
[38] B. Pompe, M. Daniel, M. Sochor, R. Vengust, V. Kralj-Iglič, A. Iglič. Gradient of contact stress in normal and dysplastic human hips. *Med. Eng. Phys*. **25**, 379–385, 2003.
[39] J. Wolff. *The law of bone remodelling*. New York. Springer, 1986.
[40] J.W. Landells. The bone cysts of osteoarthritis. *The Journal of Bone and Joint Surgery*. **35**B(4), 643-649, 1953.
[41] D. Resnick, G. Niwayama, R.D. Coutts. Subchondral Cysts (Geodes) in arthritic disorders: Pathologic and Radiographic appearance of the hip joint. *Am. J. Roentgenol.*, **128**, 799-806, 1977.
[42] H.W. Wei, S.S. Sun, S.H.E. Jao, C.R. Yeh, C.K. Cheng. The influence of mechanical properties of subchondral plate, femoral head and neck on dynamic stress distribution of the articular cartilage. *Med. Eng. Phys.* **27**, 295-304, 2004.
[43] T. Gross., D.H. Pahr, F. Peyrin, P.K. Zysset. Mineral heterogeneity has a minor influence on the apparent elastic properties of human cancellous bone: a SRμCT-based finite element study. *Computer Methods in Biomechanics and Biomedical Engineering: Imaging & Visualization*, **15**,(11), 1137-1144, 2012.
[44] F. Marinozzi, F. Bini, A. Quintino, M. Corcione, A. Marinozzi. Experimental Study of Diffusion Coefficients of Water through the Collagen–Apatite Porosity in Human Trabecular Bone Tissue. *BioMed Res. Int.*, vol. 2014, ID 796519, 8 pages, 2014
[45] F. Bini, A. Pica, A. Marinozzi, F. Marinozzi. 3D diffusion model within the collagen apatite porosity: an insight to the nanostructure of human trabecular bone. *PLoS ONE*, **12**(12), e0189041, 2017.
[46] R. Araneo, A. Rinaldi, A. Notargiacomo, F. Bini, M. Pea, S. Celozzi, F. Marinozzi and G. Lovat. Design Concepts, Fabrication and Advanced Characterization Methods of Innovative Piezoelectric Sensors Based on ZnO Nanowires. *Sensors-Basel*, **14**(12), 23539-23562, 2014
[47] R. Araneo, A. Rinaldi, A. Notargiacomo, F. Bini, F. Marinozzi, M. Pea, G. Lovat and S. Celozzi. Effect of the Scaling of the Mechanical Properties on the Performances of ZnO Piezo-Semiconductive Nanowires. *Nanoforum 2013, AIP Conf. Proc*., **1603**, 14-22. 2014.